THE ASTROPHYSICAL JOURNAL, 356:675–681, 1990 June 20

ON SOLAR RADIATION–DRIVEN SURFACE TRANSPORT OF SODIUM ATOMS AT MERCURY

W.-H. IP
Max-Planck-Institut für Aeronomie
Received 1989 September 5; accepted 1989 December 4

ABSTRACT

The ballistic motion of the exospheric sodium atoms on the surface of Mercury is modeled, taking into account the solar radiation pressure acceleration and partial surface thermal accommodation. The Monte Carlo simulations show that there should be a significant degree of limb brightening as well as brightness enhancement over the poles. To maintain the observed sodium optical emission, a surface production rate on the order of 5–9 $\times$ 10^{24} atoms s^{-1} is needed. It is also found that, under the present set of assumptions, a reasonable agreement can be reached between theoretical results and ground-based measurements for the dependence of the disk-averaged abundance of the sodium atoms on the solar radiation pressure acceleration. If the low-latitude portion of the planetary surface is shielded from the magnetospheric convective electric field, the effective loss rate of the sodium atoms via photoionization and magnetospheric pickup may be reduced to about 2 $\times$ 10^{24} atoms s^{-1}, with the polar regions acting as the main area of ion outflows.

Subject headings: planets: abundances — planets: Mercury

I. INTRODUCTION

The surprising discovery of intense sodium emission from the innermost planet Mercury by Potter and Morgan (1985) has motivated renewed interest in the origin and dynamics of this exotic planetary exosphere. Unlike the hydrogen and helium components, which could be adequately derived from the solar wind, heavy atoms such as sodium, potassium, and oxygen must come from either surface outgassing/sputtering or impact vaporization of the interplanetary meteoroids. The latter effect has been estimated to be a potential source of hot vapors (i.e., injection speed >2 km s^{-1}) with a source strength of a few times 10^{22} Na atoms s^{-1} (McGrath, Johnson, and Lanzerotti 1986; Ip 1986; Morgan, Potter, and Zook 1987). Since the strong solar radiation pressure on the Na atoms could lead to tailward acceleration of these hot atoms, the formation of an extended sodium exosphere elongated in the antisolar direction is therefore possible (Ip 1986; Smyth 1986*a*). The magnitude of the solar radiation pressure acceleration (A_{pr}) is strongly modulated by the Doppler-shift of the solar line profile. As the planet revolves around the Sun in a rather eccentric orbit ($e = 0.21$), the extension and configuration of the extended "hot" sodium exosphere should vary according to the orbital phase of Mercury (Smyth 1986*a*). In other words, when the ratio of A_{pr} to the surface gravitational force is large, then the sodium exospheric tail should be longer than the corresponding ratio at a minimum.

However, as high-resolution spectrographic measurements of the sodium emission have shown, the bulk of the sodium has a kinetic temperature (T_k) of about 500 K (Potter and Morgan 1985, 1987), which is close to the average surface temperature of the sunlit hemisphere. Any predicted change in the hot exosphere, presumably of meteoroid impact or charged particle sputtering origin, is thus difficult to discern. In any event, Potter and Morgan (1987) recently showed that the disk-averaged column abundance of sodium is inversely proportional to the magnitude of A_{pr}. A certain correlation, therefore, exists between the exospheric sodium abundance of the cold or thermal (e.g., $T_k \approx 500$ K) population and the solar radiation pressure. Potter and Morgan (1987) proposed two possible explanations:

1. During the time interval of strong solar radiation pressure, the high-speed sodium atoms from meteoroid impact could escape from the surface environment much more easily, suppressing the supply rate of sodium to the surface. This scenario, however, would be valid only if meteoroid impact vaporization were indeed the main source mechanism of the Na atoms observed. Since the loss rate of the sodium atoms via photoionization/magnetospheric acceleration could be as high as 10^{25} atoms s^{-1} (Ip 1987), much larger than the estimated supply rate from meteoroid impact, such an origin is thus by no means certain (see § III).

2. Another possibility to consider, which is somewhat decoupled from the issue of the source mechanism, is the effect of solar radiation pressure on the surface transport of the thermal component of the sodium atoms. Even though the thermal velocity corresponding to $T_k = 500$ K is only 0.6 km s^{-1}, a sodium atom could execute a sequence of random walk before it enters the nightside hemisphere. During the random walk process, the solar radiation pressure would also exert an acceleration effect in the antisolar direction. For larger values of A_{pr}, the transit time (t_{rw}) from the dayside to the nightside will be shorter. Thus, if the production rate ($\dot{N}$) of the sodium atoms is maintained constant, the total sodium abundance which is proportional to $\dot{N} \times t_{rw}$ should display a trend in qualitative agreement with the Potter and Morgan (1987) observations.

A brief account along the line of the second scenario has been given by Smyth (1986*b*) summarizing the numerical results of simulating the random walk process of sodium atoms; the accommodation coefficient for atom-surface interactions (α) was assumed to be 0 (i.e., perfectly elastic collision). Therefore, the global distribution of the exospheric number density of the sodium atoms cannot be described in terms of a surface thermal equilibrium model. Note that a new evaluation by Hunten, Morgan, and Shemansky (1988) produced a number of $\alpha \approx 0.5$–0.6. In other words, the Hunten, Morgan, and Shemansky value requires about half the kinetic energy of the sodium atoms be accommodated by the surface at impacts. Taking Smyth (1986*b*) as a guide, we shall make a numerical simulation of the solar radiation–driven surface transport of

thermal sodium atoms across the planetary surface—one which lies intermediate between complete thermal equilibrium ($\alpha \approx 1$) and perfectly elastic atom-surface collision. Three issues are to be explored:

a) the surface column density (and brightness) distribution of the sodium emission over the sunlit hemisphere;

b) the effect of spatial distribution of the sodium surface production rate on the column density distribution;

c) the dependence of the sodium abundance on Mercury's orbital phase around the Sun.

II. NUMERICAL SIMULATIONS

The principal formation of the Monte Carlo model used here is similar to the one developed in an earlier work on the ballistic motion of Na atoms in the vicinity of Mercury (Ip 1986). The basic steps in our modeling involve tracking of the particle motion for a total of K test particles. The launch of the test particles is random in different directions. The trajectory calculations at integration time step Δt are performed by including the solar radiation pressure acceleration A_{pr} assumed to be constant in individual case studies. The initial speed is given by

$$u_0 = (2k_B T_0/m)^{1/2} , \quad (1)$$

where k_B is the Boltzmann constant and T_0 is the surface temperature at the injection site. Hence, in the present work we will neglect the details of the velocity distribution of the ejected particles. The surface temperature is approximated by $T(\theta, \phi) = 545(\sin\theta \cos\phi)^{1/4}$ at longitude ϕ and colatitude θ on the dayside hemisphere. The sodium atoms are traced until they move across the terminator (hence, in this paper the nightside hemisphere is assumed to be a sink for the sodium atoms). In the present thermal model, the surface temperature profile is symmetric in respect to the Sun-planet line. (In a more realistic situation in which the effect of the thermal inertia is to be taken into consideration, the axial symmetry will be broken and be replaced by a north-south asymmetry.) The contribution of the kth particle to the projected column density or surface brightness at integration time $t_p = (p\,\Delta t)$ is then given by the weighting function

$$f_k(t_p) = \exp(-t_p/t_i) , \quad (2)$$

where t_i is the photoionization time scale. The total column density distribution is then represented by the summations of all $f_k(t)$ values in the corresponding bins of projected surface areas. In other words, we have the following expression for the surface column density of the sodium atoms at the sth bin:

$$N_s = C \sum_K \sum_p f_K(t_p) , \quad (3)$$

with the corresponding values of x_p^k and y_p^k contained in the sth rectangular bin. In equation (3), C is a scaling factor. The surface number density at the same point is then given by $n_s = N_s/A_s$, where A_s is the surface area on the hemispherical surface.

Concerning the problem of surface thermal accommodation, we assume that at rebound of the jth surface impact ($j = 1, 2, 3\ldots$), the ejection speed is given by

$$v_j = [\alpha u_j^2 + (1 - \alpha)v_{j-1}^2]^{1/2} , \quad (4)$$

where $\alpha = 0.5$, v_{j-1} is the incoming speed of the particle at surface impact, and $u_j = (2k_B T_j/m)^{1/2}$ is the thermal speed at the jth impact site with surface temperature T_j.

The relation given in equation (4) may not be the most realistic representation of the surface thermal accommodation effect of the sodium atoms. One should also take note of the fact that the relevant atom-surface interactions may partly be determined by microstructures of the surface regolith (see Hapke and Cassidy 1978) which could be conductive to multiple scattering or temporal trapping of the Na atoms in the cavities of the "fairy-castle" structures of the surface dust layer. The main purpose of equation (4), however, is to say that the atom-surface interaction should not be characterized by perfectly elastic collision (i.e., $\alpha \approx 0$)—as pointed out by Hunten, Morgan, and Shemansky (1988). A more accurate expression is still to be investigated (D. Shemansky 1988, private communication).

As studied before by Smyth (1986*a*), the solar radiation pressure accelerations of the sodium and potassium atoms are quite sensitive to the orbital phase of Mercury. The physical situation can be understood most clearly by examining the curve of A_{pr} (Na) in Figure 1. Also shown are the corresponding photoionization time scales of the sodium atom. Because of the radial variations of the t_i values, the total abundance of the exospheric sodium (and potassium) atoms would not behave solely as a function of the solar radiation pressure acceleration. Before discussing this point in detail, we would like to consider a few numerical runs with different combinations of t_i and A_{pr}

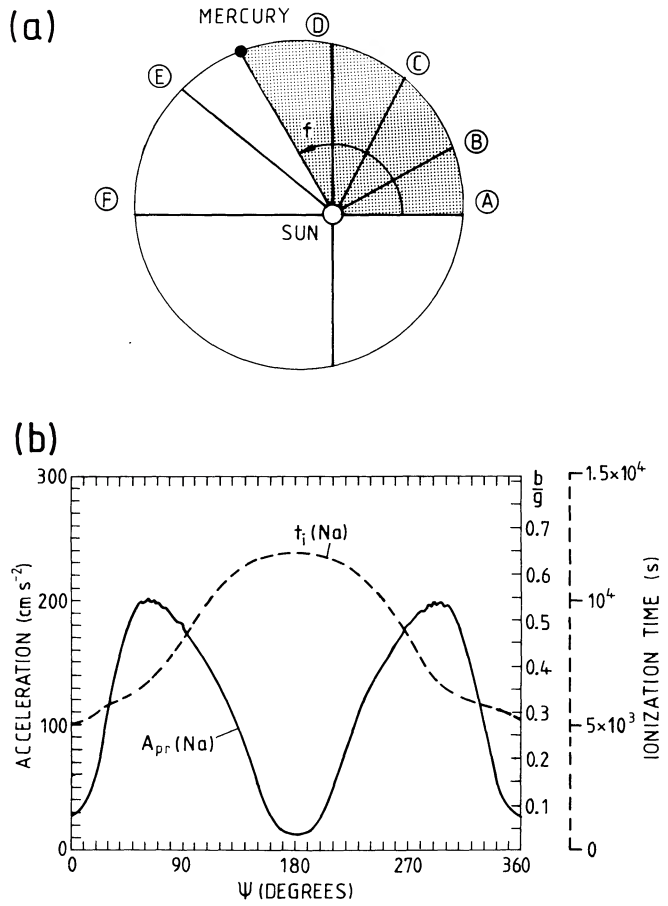

FIG. 1.—Variations of the solar radiation pressure acceleration of the sodium atom and the corresponding photoionization time scale as functions of the orbital phase of Mercury (*a*). Value of A_{pr}(Na) is from Smyth (1986*a*) (*b*).

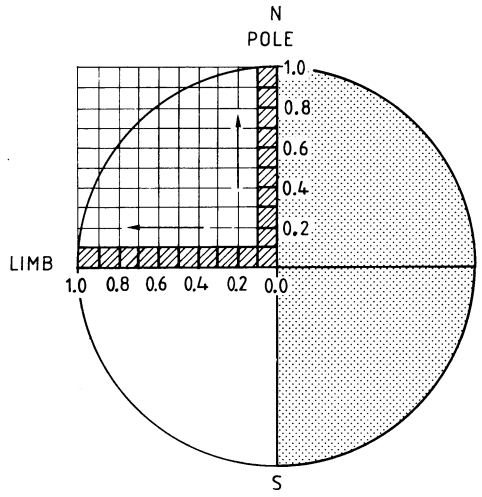

FIG. 2.—The computational scheme in the binning of the test particles. The shaded regions denote the two arrays used in estimating the center-to-pole and center-to-limb variations of the column and surface densities. In the determination of the projected column density, the rectangular bins are configurated in such a way that the projection axis is always parallel to the line of sight.

so that the general behavior of the surface column density distribution may be understood.

a) Surface Column Density Distribution

For the case studies, we have employed $K = 5000$ test particles in each run. Assuming an idealized viewing geometry with the line of sight perpendicular to the Earth-planet line, we shall perform the summation procedure in 10×10 bins (i.e., 1 bin $= 244 \times 244$ km^2) for one quadrant projected on the dayside hemisphere (see Fig. 2). Two surface distributions of the source strength of the sodium atoms are considered:

a) uniform production rate on the sunlit hemisphere, and

b) production rate following a cosine law of the solar insolation angle.

The summary plots for the cases of maximum solar radiation pressure acceleration ($A_{pr} = 200$ cm s^{-2}) and for minimum value ($A_{pr} = 30$ cm s^{-2}) are illustrated in the gray-toned figures (Fig. 3). To be noted are the limb-enhancement effect as well as the tendency for increased column density near the pole, when scanned in a north-south orientation. Both effects basically result from projection.

A comparison of the cases with different values of A_{pr} and t_i also shows that the limb-enhancement effect is increased when the solar radiation pressure is at a minimum. In total, six combinations (A–F) of A_{pr} and t_i pertinent to different locations along Mercury's orbit (see Fig. 1) have been considered. A quantitative description can be seen in Figure 4 for the surface column densities along the center-to-pole and the center-to-limb directions. In general, there are visible differences in the distributions of the surface column densities for the two surface distributions of the sodium source rate [i.e., (*a*) uniform distribution and (*b*) cosine distribution]. As a result of viewing geometry, the surface column density distribution projected on the planetary disk would exhibit a certain enhancement (a factor of 4) at the poles in comparison with the value near the planetary center.

It is also interesting to examine briefly the statistics of the ballistic transport process. With the case (C) as an example, Figure 5 illustrates the histograms for the distributions of the ballistic velocity of the sodium atoms across the planetary hemisphere as well as the transient time that is required for the sodium atoms to move into the nightside. The distribution of the ballistic velocity peaks at about 0.5 km s^{-1} with a sharp cutoff at about 1.7 km s^{-1}. The average value of the transit time is 5.7×10^3 s. The total cumulative time steps for the 5000 test particles is 3.69×10^6.

The actual surface production of sodium atoms could in fact be patchy and localized according to the geochemical provinces on Mercury's surface, and furthermore, the magnetospheric loss process due to pickup of the photoions from the exosphere could introduce both spatial and temporal variations. Therefore one would not expect the sodium abundance variations as inferred from observations to yield results to agree with the present theoretical profiles which are produced with the simplest set of assumptions. On the other hand, the numerical model calculations as discussed here could be the basis for interpretation and further improvement for imaging and spectrographic work. For example, observations of the resonantly scattered sodium emission from Mercury in the last few years have suggested that the effect of a slight polar brightening indeed existed for both sodium and potassium emissions (Tyler *et al.* 1986; Tyler, Kozlowski, and Schneider 1987; A.L. Tyler, 1988, private communication; R. M. Killen 1988, private communication). One possible outcome of our modeling effort would be to understand the interrelation between source and sink of the sodium atoms, and the magnetospheric effect of controlling the ballistic transport of the exospheric particles.

b) Time Variation of Global Exospheric Sodium Abundance

To scale the numerical values in our simulations to the actual numbers at Mercury, we recall that the total number of test particles in each run is $K = 5000$ and that the integration time step in the trajectory calculation is $\Delta t = 5$ s. Taking the value at orbital phase C as an example, we find that the disk-averaged column density from the theoretical calculations for the case of uniform source distribution is

$$N_t = 3.69 \times 10^6/A = 1.97 \times 10^{-11} \text{ number of } \Delta t - \text{time steps cm}^{-2}, \quad (5)$$

where $A = \pi R_p^2$ with $R_p (= 2440$ km) as the planetary radius. Since the observed value for the disk-averaged column density is $N_0 = 1.07 \times 10^{11}$ atoms cm^{-2} (Potter and Morgan 1987), the corresponding ratio is therefore

$$\xi = \frac{N_0}{N_t} = 5.4 \times 10^{21}, \quad (6)$$

and the resulting production rate is

$$\dot{N} = \xi(K/\Delta t) = 5.4 \times 10^{24} \text{ atoms s}^{-1}. \quad (7)$$

In the case of a cosine source distribution, the theoretical value of N_t is 1.26×10^{-11} particles cm^{-2} and $\xi = 8.5 \times 10^{21}$. The corresponding surface production rate of sodium atoms is thus $\dot{N} = 8.5 \times 10^{24}$ atoms s^{-1}.

Such large values of the sodium production rate are unmatched by source mechanisms examined so far. This is one issue which has to be investigated closely. The other issue has to do with the effective loss rate of the sodium atoms. The photoionization rate can be estimated to be $\dot{N}_i \approx 2AN_0/t_i$ or about 6.3×10^{24} atoms s^{-1}. Only if most of the ionized sodium atoms could be recycled back to the planetary surface, the required rate of replenishment would be much less than

10^{24} atoms s^{-1}. In this event, the sum of meteoroid impact, photosputtering, and thermal emission could be adequate in accounting for the observed sodium optical emission (McGrath, Johnson, and Lanzerotti 1986; Hunten, Morgan, and Shemansky 1988).

Since the most rapid loss of the exospheric sodium atoms is directly connected to the magnetospheric pickup process of photoions (Ip 1987), it is possible that the loss rate may be reduced if an efficient shielding of the magnetospheric electric field to a distance of about 50–100 km above the planetary surface could exist such that the sodium ions could immediately return to the planetary surface after creation. Even though the very tenuous nature of the Mercurian exosphere does not permit the buildup of a sufficiently high ionospheric conductivity, the antisunward drifts of the electrons and ions in the magnetotail resulting from the cross-tail electric field might produce significant charge separation effect in the inner magnetosphere such that the convective field is partly screened. In this event, only the polar cap region will be directly mapped by the cross-tail electric field. Suppose the latitude of the polar cap is at 45°; about 30% of the exospheric sodium atoms are still subject to loss via magnetospheric pickup immediately after photoionization. The effective sodium loss rate hence is still on the order of 2×10^{24} atoms s^{-1}.

Next, to examine the large-scale variation in the sodium abundance as a function of the orbital phase of Mercury, the total column densities obtained in different case studies are normalized to the observed values from Potter and Morgan (1987). As shown in Figure 6, if the total production rate is independent of the solar distance (r), there is a clear bifurcation

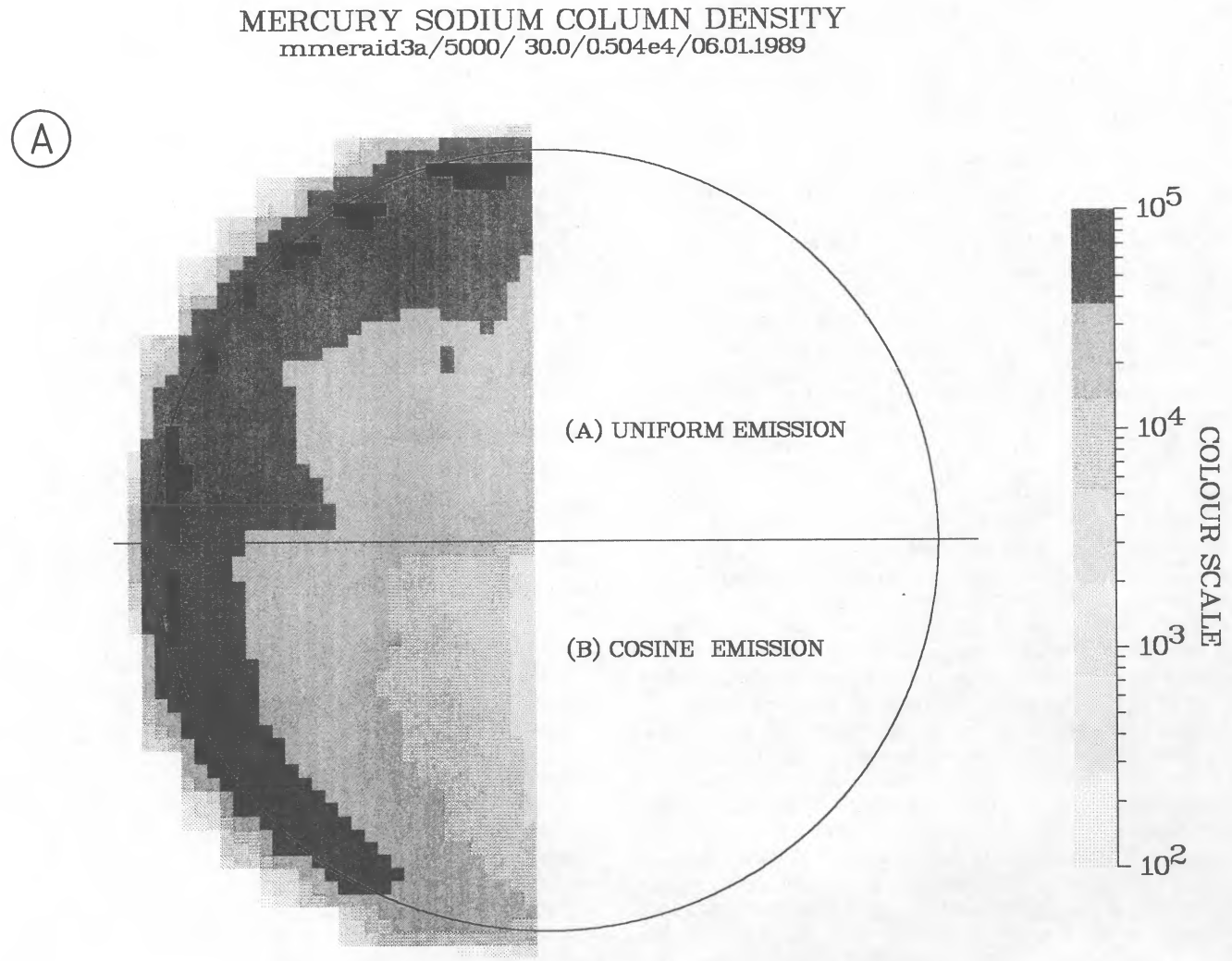

FIG. 3a

FIG. 3.—The gray-toned pictures of the surface brightness (and projected column density) distributions of the sodium atoms: (*a*) $A_{pr} = 30$ cm s^{-2} and $t_i = 5000$ s; (*b*) $A_{pr} = 200$ cm s^{-2} and $t_i = 6300$ s.

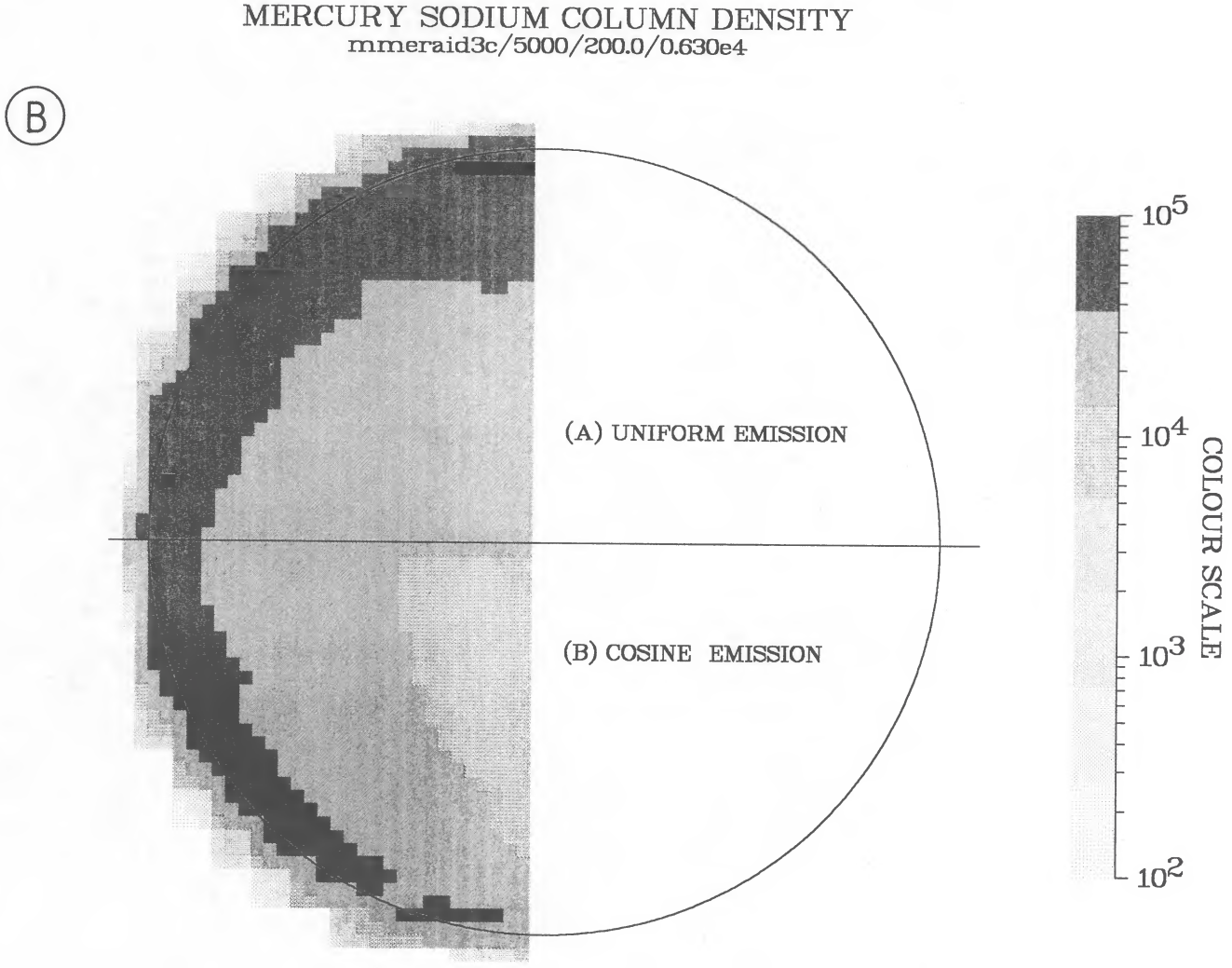

FIG. 3*b*

of the data points connecting from A to C and from C to F. The reason is, simply, that the photoionization time scale is considerably shorter on the lower branch than that on the upper branch (see Fig. 1). The difference of a factor of 2.3 is reflected in the ratio of the column density at point F and that at point A. From this point of view, our present theoretical results appear to just bracket the data points from ground-based measurements. However, if we assume that the intrinsic production rate of sodium atoms from the surface of Mercury is also a function of r, then the theoretical profiles could vary accordingly. For example, if photosputtering is a major source mechanism, the sodium production rate will be proportional to $1/r^2$. The modifications to the theoretical column surface densities in Figure 6 demonstrate that better agreement may indeed result.

III. DISCUSSION

Using a rather simple set of assumptions, we have investigated some basic properties of the solar radiation-driven surface transport of sodium atoms at Mercury. In uniform and cosine surface distributions of the sodium production rate, we found both the limb enhancement (for east-west scans) of the surface column abundance and a similar effect in the polar region (for north-south scans). The theoretical surface column density profiles for center-to-pole and center-to-limb scans might thus be used to infer the surface distribution of the sodium production. For example, for both thermal release and photosputtering processes, we would expect the cosine production law to be more appropriate. At the same time, the dependence of the global production rate on the solar distance can also be examined by comparing the surface column densities (or optical brightnesses) measured at different orbital phases of the planet. The present work, with its array of diagnostic possibilities, points to a promising way of quantitative study of the sodium (and potassium) production from Mercury.

Note that in a more detailed investigation, the problem of radiative transfer may have to be coupled with the ballistic transport process. This is because the sodium emission could be optically thick in the exospheric layer (Potter and Morgan

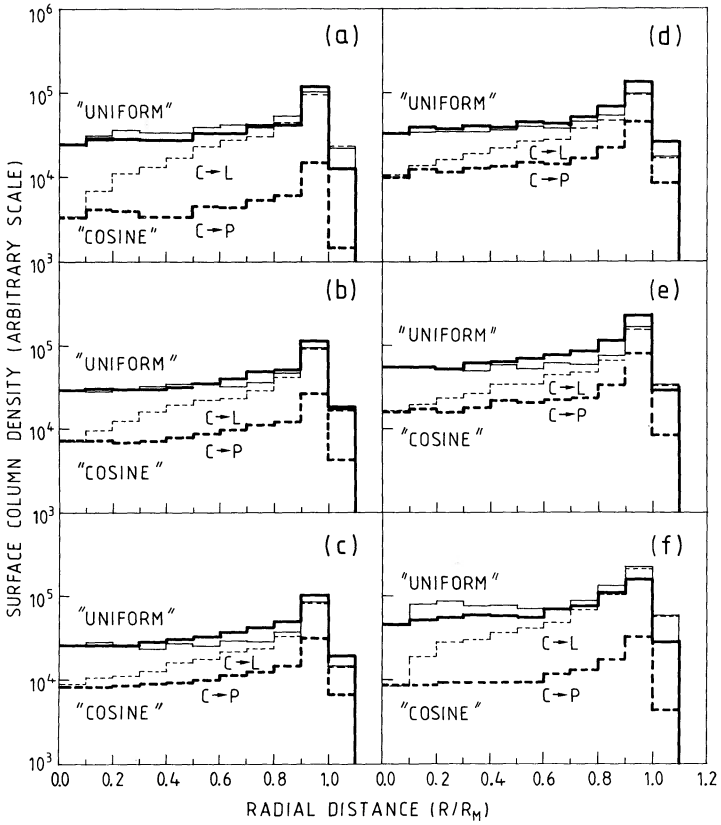

FIG. 4

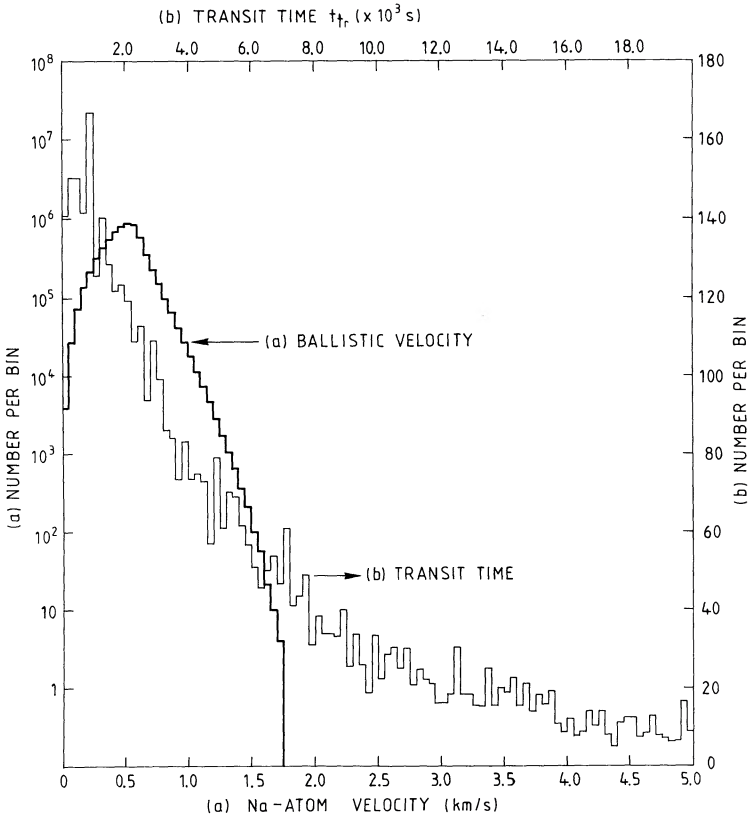

FIG. 5

FIG. 4.—Center-to-pole scans (*thick curves*) and center-to-limb scans (*thin curves*) of the projected surface column densities of the sodium atoms. (*a*) $A_{pr} = 30$ cm s^{-2}, $t_i = 5.0 \times 10^3$ s. (*b*) $A_{pr} = 110.0$ cm s^{-2}, $t_i = 5.4 \times 10^3$ s. (*c*) $A_{pr} = 200.0$ cm s^{-2}, $t_i = 6.3 \times 10^3$ s. (*d*) $A_{pr} = 170.0$ cm s^{-2}, $t_i = 8.3 \times 10^3$ s. (*e*) $A_{pr} = 90.0$ cm s^{-2}, $t_i = 1.1 \times 10^4$ s. (*f*) $A_{pr} = 15.0$ cm s^{-2}, $t_i = 1.2 \times 10^4$ s. The model of uniform source distribution is marked by solid curves, and the model for cosine source distribution is marked by dashed curves.

FIG. 5.—The histograms for the distributions of the ballistic velocity and transit time of the sodium atoms during their random walks across the dayside hemisphere. The examples given are for case C with solar pressure acceleration $A_{pr} = 200$ cm s^{-2} and photoionization time scale of $t_i = 6.3 \times 10^3$ s.

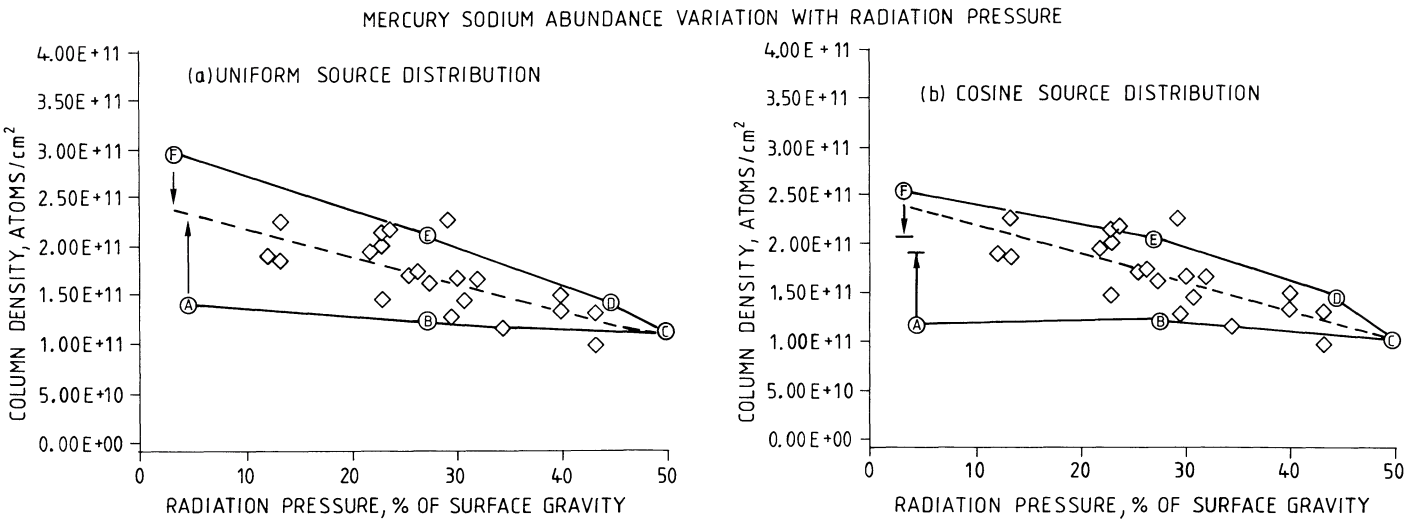

FIG. 6.—A comparison of the observed values of the disk-averaged column abundance of the sodium atoms (diamonds from Potter and Morgan 1987) with the theoretical results (A–F) as functions of the radiation pressure acceleration and orbital phase: (*a*) uniform surface distribution and (*b*) cosine emission distribution. The modifications obtained by inclusion of an $1/r^2$ dependence of the intrinsic sodium emission rate are indicated by the arrows.

1987; Killen 1988). The effective radiation pressure on the sodium atoms might not be as constant and unidirectional as considered here. Another uncertainty deals with the effective loss rate of the sodium atoms, which we have identified to be very sensitive to the penetration of the magnetospheric electric field to the surface environment of the planet.

We discussed how the magnetospheric pickup loss may be reduced by screening the planetary surface from the convective electric field. However, the polar cap regions which are magnetically connected to the magnetotail would still permit a loss rate of about 2×10^{24} Na atoms s^{-1}. Since the Lorentz forces depend on the magnitude of the convective electric field as well as on the magnetic field distribution in these localized regions, the value of 2×10^{24} atoms s^{-1} may be considered as a lower limit of the sodium loss rate. In this scenario, one would expect sodium atoms to be generated by solar UV radiation and ion sputtering on the dayside, and then be driven to the nightside hemisphere. Once inside the polar cap regime, the ionized sodium atoms could be accelerated away from the planetary surface by the magnetospheric convective electric fields. A jet of Na^+, K^+, and Mg^+ ion flow might possibly form and be detected by a Mercury Polar Orbiter as it passes one of the poles. The generation of such a polar jet of heavy metallic ions should be more frequent during substorm intervals, since the convective electric field is enhanced in those periods. On the other hand, the electrostatic charging of the planetary surface by the precipitating charged particles could, in principle, also influence the ejection efficiency of the photoions. These interrelated dynamical processes are to be investigated in a future work.

We wish to thank D. M. Hunten, R. M. Killen, T. Morgan, A. Potter, D. Shemansky, W. H. Smyth, and Ann Tyler for useful discussions and information. Comments by W. H. Smyth were also very useful in improving the content of this paper. A part of the paper was presented at the XIII General Assembly of the European Geophysical Society at Bologna, Italy, 1988 March 21–25.

REFERENCES

Hapke, B., and Cassidy, W. 1978, *Geophys. Res. Letters*, **5**, 297.
Hunten, D. M., Morgan, T. M., and Shemansky, D. E. 1988, in *Mercury*, ed. F. Vilas, C. R. Chapman, and M. S. Matthews (Tucson: University of Arizona Press), p. 561.
Ip, W.-H. 1986, *Geophys. Res. Letters*, **13**, 423.
———. 1987, *Icarus*, **71**, 441.
Killen, R. M. 1988, *Geophys. Res. Letters*, **15**, 80.
McGrath, M. A., Johnson, R. E., and Lanzerotti, L. J. 1986, *Nature*, **323**, 694.
Morgan, T. H., Potter, A. E., and Zook, H. A. 1987, in *Proc. 18th Lunar Planet. Sci. Conf.* (NASA: Lunar and Planetary Institute), pp. 663–664.
Potter, A. and Morgan, T. 1985, *Science*, **229**, 651.
———. 1986, *Icarus*, **67**, 336.
———. 1987, *Icarus*, **71**, 472.
Smyth, W. H. 1986*a*, *Nature*, **323**, 696.
———. 1986*b*, paper presented at The Mercury Conference, Tucson, Arizona.
Tyler, A. L., Kozlowski, R. W., and Schneider, N. M. 1987. *Bull. AAS*, **19**, No. 3, 862.
Tyler, A. L., Schneider, N. M., Wells, W. K., Hunten, D. M., and Kozlowski, R. W. H. 1986, *Bull. AAS*, **18**, No. 3, 781.

W.-H. IP: Max-Planck-Institut für Aeronomie, Postfach 20, D-3411 Katlenburg-Lindau, Federal Republic of Germany